

Contents

2	1	Charge monitoring	2
3		<i>The ATLAS Diamond Beam Monitor</i>	2
4	1.1	Luminosity measurements	3
5	1.2	Diamond pixel module	4
6	1.2.1	Sensors	5
7	1.2.2	Front-end electronics	6
8	1.3	Module assembly and quality control	8
9	1.3.1	Assembly	8
10	1.3.2	Testing	9
11	1.3.3	Installation and commissioning	10
12	1.4	Performance results	11
13	1.4.1	Source tests	11
14	1.4.2	Test beam results	12
15	1.5	Operation	14
16	1.5.1	Positioning	14
17	1.5.2	Data taking during collisions	15
18	1.6	Conclusion	18

¹⁹ **Chapter 1**

²⁰ **Charge monitoring**

²¹ *The ATLAS Diamond Beam Monitor*

²² Particle detectors in high energy physics experiments need to meet very stringent
²³ specifications, depending on the functionality and their position in the experiment.
²⁴ In particular, the detectors close to the collision point are subject to high levels of
²⁵ radiation. Then, they need to operate with a high spatial and temporal segmentation
²⁶ to be able to precisely measure trajectories of hundreds of particles in very short
²⁷ time. In addition, they need to be highly efficient. In terms of the structure, their
²⁸ active sensing material has to be thin so as not to cause the particles to scatter
²⁹ or get stopped, which would worsen the measurements. This also means that they
³⁰ have to have a low heat dissipation so that the cooling system dimensions can be
³¹ minimised. Finally, they need to be able to operate stably for several years without
³² an intervention, because they are buried deep under tonnes of material and electronics.

³³ The material of choice for the inner detector layers in the HEP experiments is
³⁴ silicon. It can withstand relatively high doses of radiation, it is highly efficient (of the
³⁵ order of $\sim 99.9\%$) and relatively low cost due to using existing industrial processes
³⁶ for its production. Its downside is that, with increasing irradiation levels, it needs to
³⁷ be cooled to increasingly low temperatures to ensure a stable operation. This is not
³⁸ the case with diamond. In addition, diamond has a lower radiation damage factor,
³⁹ which means it can operate in a radiation-heavy environment for a longer period.

⁴⁰ The ATLAS Diamond Beam Monitor (DBM) [] is a novel high energy charged
⁴¹ particle detector. Its function is to measure luminosity and beam background in the
⁴² ATLAS experiment. Given its position in a region with a high radiation dose, di-
⁴³ amond was chosen as the sensing material. The monitor's pCVD diamond sensors
⁴⁴ are instrumented with pixellated FE-I4 front-end chips. The pCVD diamond sensor
⁴⁵ material was chosen to ensure the durability of the sensors in a radiation-hard envi-
⁴⁶ ronment and the size of its active area. The DBM is not the first diamond detector
⁴⁷ used in HEP, but it is the largest pixellated detector installed so far (see figure 1.1).
⁴⁸ It was designed as an upgrade to the existing luminosity monitor called the Beam
⁴⁹ Conditions Monitor (BCM) [] consisting of eight diamond pad detectors, which is

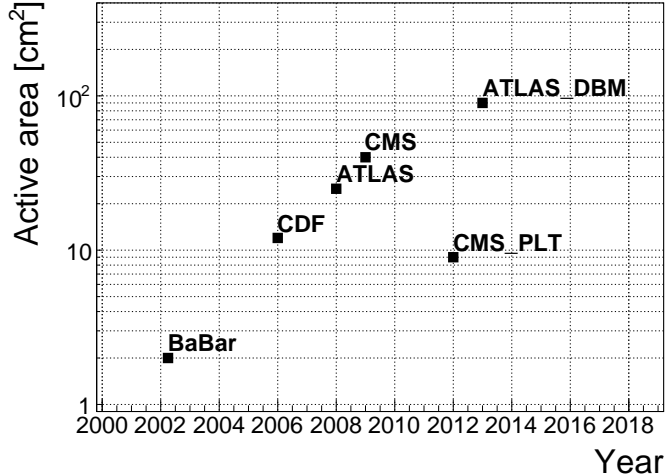


Figure 1.1: Diamond detectors installed in high-energy physics experiments in the last decade, sorted by the active sensor area. The first four detectors from the left are radiation monitors whereas the right two are pixel trackers.

able to perform precise time-of-flight (ToF) measurements. The DBM complements the BCM's features by implementing tracking capability. Its pixelated front-end electronics significantly increase the spatial resolution of the system. Furthermore, the DBM is able to distinguish particle tracks originating in the collision region from the background hits. This capability is a result of its projective geometry pointing towards the interaction region. This chapter first describes the principles of luminosity measurements. It then explains how the DBM will carry out this task. Finally, some results from tests and from the real collisions are presented.

When a particle traverses a sensor plane, a hit is recorded in the corresponding pixel. Thus, a precise spatial and timing information of the hit is extracted. With three or more sensors stacked one behind the other, it is also possible to define the particle's trajectory. This is the case with the DBM. Its projective geometry allows the particles to be tracked if they traverse the sensor planes. The DBM relates the luminosity to the number of particle tracks that originate from the collision region of the ATLAS experiment. Particles that hit the DBM from other directions are rejected as background radiation.

1.1 Luminosity measurements

Luminosity is one of the most important parameters of a particle collider. It is a measurement of the rate of particle collisions that are produced by two particle beams. It can be described as a function of beam parameters, such as: the number of colliding bunch pairs, the revolution frequency, the number of particles in each bunch and the transverse bunch dimensions. The first four parameters are well defined. However, the transverse bunch dimensions have to be determined experimentally

1.2. DIAMOND PIXEL MODULE

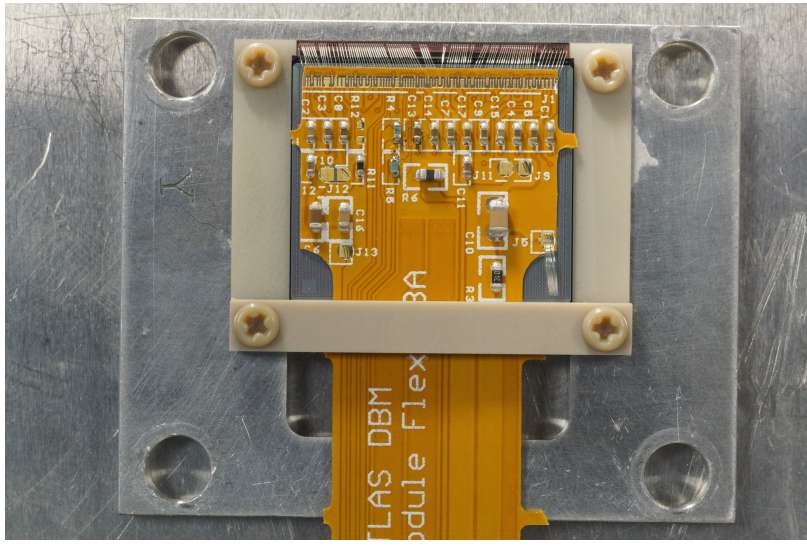


Figure 1.2: DBM module, top-down view. Visible is the flexible PCB with signal and power connections, the silicon sensor and a part of the FE-I4. Wire bonds from the PCB to the FE-I4 and to the sensor are also visible.

73 during calibration. The ATLAS experiment uses the *van der Meer scan* [1] during
74 low-luminosity runs to calibrate the luminosity detectors. This scan is performed
75 by displacing one beam in a given direction and measuring the rate of interactions
76 as a function of the displacement. Transverse charge density of the bunches can be
77 estimated on the basis of the interaction rate. The calibrated luminosity detectors
78 can then operate during high-luminosity runs.

79 One approach to luminosity monitoring is to count the number of particles pro-
80 duced by the collisions. The luminosity is then proportional to the number of detected
81 particles. A detector has to be capable of distinguishing individual particles that fly
82 from the interaction point through the active sensor area. If the detector has at least
83 three layers, it can reconstruct the particles' tracks, which in turn yields more infor-
84 mation on their trajectory. This is one reason why detectors with a high timing-
85 and spatial segmentation are more suitable for these applications. The second reason
86 is that, with a high spatial segmentation, the detector will not saturate even at high
87 particle fluencies.

88 1.2 Diamond pixel module

89 The two most important parts of the diamond pixel module (seen in figure 1.2) are
90 the sensor, which detects ionising radiation, and the pixellated front-end chip, which
91 collects the ionised charge with a high spatial segmentation, processes the recorded
92 data and sends them to the readout system. This section describes these two main
93 parts of the module and their interconnection.

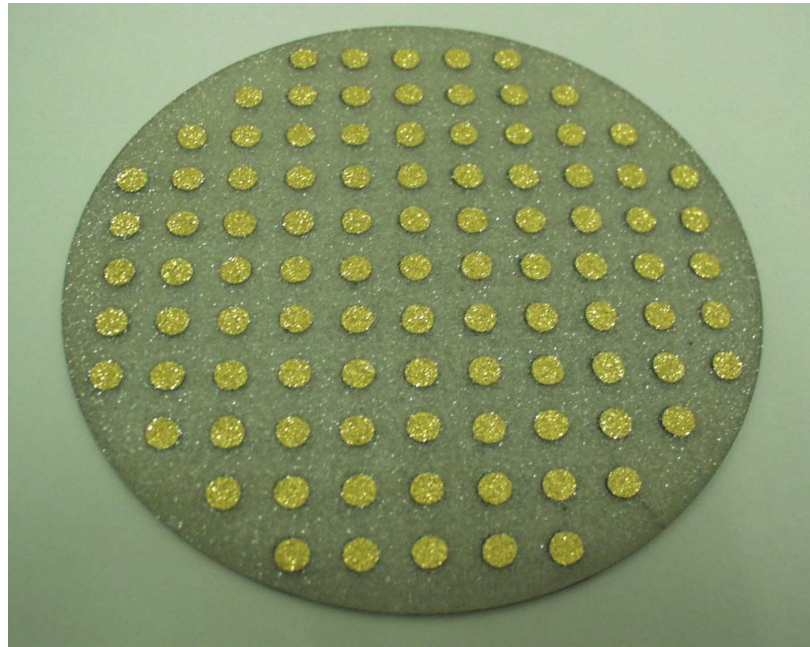


Figure 1.3: A pCVD wafer. The golden dots on the surface are the electrodes that are applied during the qualification test. The wafer is measured across the surface to find the regions with the highest efficiency.

⁹⁴ **1.2.1 Sensors**

⁹⁵ The DBM modules are instrumented with two types of sensors – pCVD diamond and
⁹⁶ silicon. The silicon sensors are used as a fallback solution because there were simply
⁹⁷ not enough high-quality diamond sensors available. In addition, a comparative study
⁹⁸ of irradiation damage between silicon and diamond can be made with such a hybrid
⁹⁹ system.

¹⁰⁰ **Diamond sensors** The target material for this application is pVCD diamond. The
¹⁰¹ reason for this is that the active area of an individual sensor must be approximately
¹⁰² 4 cm^2 , which is too large for the sCVD diamond. pCVD material is also a bit
¹⁰³ cheaper, which makes a detector with a large active area more feasible to build. The
¹⁰⁴ material is provided by three companies: DDL, E6 and II-IV and it is grown in
¹⁰⁵ 15 cm wafers, as seen in figure 1.3. The target thickness of the wafers is 500 μm and
¹⁰⁶ the minimum required charge collection efficiency is 40 % ($\text{CCD} \geq 200 \mu\text{m}$). They
¹⁰⁷ need to be operated at bias voltages between 600–1000 V. On one side there is a
¹⁰⁸ single gold electrode applied across the whole surface. On the other side a pixellated
¹⁰⁹ metallisation is added.

¹¹⁰ **Silicon sensors** are standard $n^+ - in - n$ planar sensors with a 200 μm thickness
¹¹¹ and were mostly fabricated at CiS [], a company from Erfurt, Germany. They are
¹¹² designed to have nearly a 100 % efficiency when non-irradiated. Their bulk resistivity
¹¹³ is between 2–5 $\text{k}\Omega\text{cm}$ and they were diffusion oxygenated at 1150 °C for 24 hours to

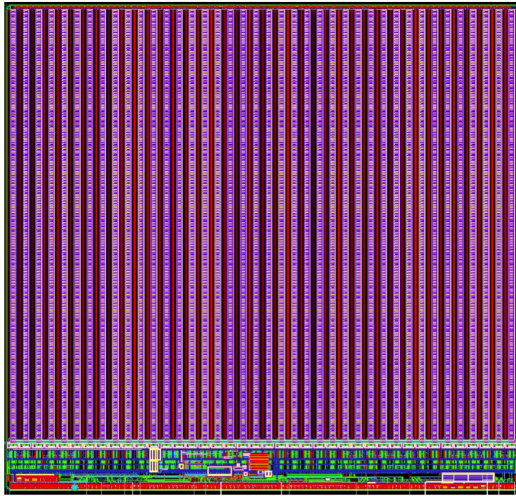


Figure 1.4: FE-I4 layout, top-down view. The pink area are pixels grouped into columns, the green area below is the common logic and the red strip at the bottom are the wire bond pads.

114 increase their radiation hardness. One side is segmented into pixels. Guard rings at
115 the edges of the sensor provide a controlled drop in potential, reducing the possibility
116 of shorts at maximum design bias voltages of the order of 1000 V.

117 1.2.2 Front-end electronics

118 The FE-I4 (front-end version four) [1] is an ASIC pixel chip designed specifically for
119 the ATLAS pixel detector upgrade. It is built as a successor to the current pixel chip
120 FE-I3, surpassing it in size of the active area ($4\times$ larger) as well as the number of
121 channels/pixels ($10\times$ more). 336 such FE-I4 modules are used in the newly installed
122 pixel layer called the Insertable B-Layer (IBL) [2]. The DBM is also instrumented
123 with these chips. The FE-I4's integrated circuit contains readout circuitry for 26880
124 pixels arranged in 80 columns on a $250\text{ }\mu\text{m}$ pitch and 336 rows on a $50\text{ }\mu\text{m}$ pitch. The
125 size of the active area is therefore $20.0\times16.8\text{ mm}^2$. This fine granularity allows for a
126 high-precision particle tracking. The chip operates at 40 MHz with a 25 ns acquisition
127 window, which corresponds to the spacing of the particle bunches in the LHC. It is
128 hence able to correlate hits/tracks to their corresponding bunch. Furthermore, each
129 pixel is capable of measuring the deposited charge of a detected particle by using
130 the Time-over-Threshold (ToT) method. Finally, the FEI4 has been designed to
131 withstand a radiation dose up to 300 MGy. This ensures a longterm stability in the
132 radiation hard forward region of the ATLAS experiment.

133 Each pixel is designed as a separate entity. Its electrical chain is shown in fig-
134 ure 1.5. The bump-bond pad – the connection to the outside of the chip – is the
135 input of the electrical chain, connected to a free-running amplification stage with ad-
136 justable shaping using a 4-bit register at the feedback branch. The analog amplifier is
137 designed to collect negative charge, therefore electrons. The output is routed through

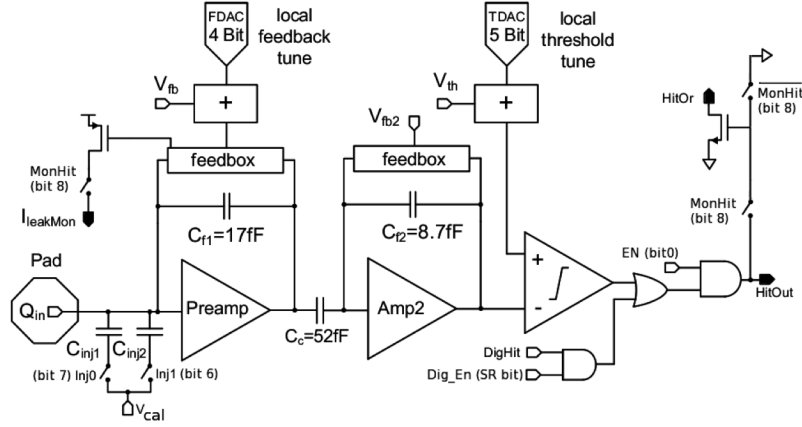


Figure 1.5: Schematic of an analog pixel. Courtesy of the FE-I4 collaboration.

138 a discriminator with an adjustable threshold. This value in effect defines the level at
 139 which the circuit will detect a hit. In addition, there is a counter of the clock cycles
 140 (25 ns sampling) during which the signal is above the discriminator threshold. The
 141 value of the counter is proportional to the collected charge. The logic gates at the end
 142 of the chain are used to enable/disable the pixel and to issue a so-called HitOr flag –
 143 this signal is set whenever at least one of the pixels was hit and is used as a trigger
 144 for the readout. The output of the chain – HitOut – is routed into the logic of the
 145 chip where it is buffered and eventually sent out to the readout system. The module
 146 receives all its commands from the system via a 40 MHz LVDS line. The commands
 147 are either settings for the pixel registers or triggers that start the data readout. The
 148 data are sent via an LVDS line at up to 320 Mbit/s, but by default at 160 Mbit/s,
 149 four times faster than the clock of the device. This allows the chip to clear out its
 150 buffers before new data are recorded, thus avoiding dead time and data pile-up. The
 151 FE-I4 has been successfully tested for trigger rates of up to 300 kHz.

152 The DBM uses pCVD diamond with $d_C = 500 \mu\text{m}$ thickness and silicon with
 153 $d_{Si} = 200 \mu\text{m}$ thickness as a sensor material. The resulting most probable value
 154 (MPV) of the deposited charge for a minimum ionising particle (MIP) is calculated
 155 with the formula $Q_S = d \cdot E_{e-h}$ and equals 18000 electrons and 17800 electrons,
 156 respectively, at a full charge collection efficiency. Unfortunately this is not the case
 157 with the pCVD material, whereby the expected charge collection efficiency is of the
 158 order of 50 % – around 9000 e. This value further decreases with received irradiation
 159 dose. Therefore in order to detect the particles depositing energy on the far left side
 160 of the landau spectrum, the threshold has to be set to a significantly lower value.
 161 On the other hand, if the threshold set too low, it also detects the electronic noise
 162 and stores a false noisy hit. With the typical noise amplitudes being in the range of
 163 120–200 e, a safe threshold range would be between $Th = 1000\text{--}3000$ e. The target
 164 for the DBM is to lower the threshold down to 800 e.

165 The analog amplifier is implemented in two stages to get a fast rise time at a low
 166 noise and a low power consumption. The output signal of the analog amplifier has a

1.3. MODULE ASSEMBLY AND QUALITY CONTROL

triangular shape with a fast rise time and a long decay. The shape can be adjusted by tuning the amplifier feedback loop. Its length is proportional to the collected charge, but it needs to be calibrated first. This is done by means of two injection capacitors, $C_{\text{inj}1}$ and $C_{\text{inj}2}$, seen in figure 1.5 with well defined capacitances. First, the charge $Q_{\text{cal}} = V_{\text{cal}} \cdot (C_{\text{inj}1} + C_{\text{inj}2})$ is injected into the analog chain. Then the length of the output pulse is measured and finally the feedback value is changed to either lengthen or shorten the pulse in order to get to the required duration t_{cal} . The typical values are $Q_{\text{cal}} = 5000 - 16000$ e at the time $t_{\text{cal}} = 5 - 10$ ToT. The target values depend on the sensor, the type of a radioactive source and the application. Therefore the initial threshold Th at 1 ToT and the calibrated value Q_{cal} at t_{cal} ToT give us a linear scale of collected charge with respect to time over threshold. However, in practice this relation is nonlinear for lower thresholds, but since the goal of the measurements is to track the particles rather than to measure their deposited energy precisely, this is sufficient.

1.3 Module assembly and quality control

Parts for the detector arrived separately and were assembled into modules at CERN’s DSF lab after being checked for production faults. The assembled modules underwent a series of quality control (QC) and burn-in tests to determine their quality, efficiency and long-term stability.

1.3.1 Assembly

A single-chip module consists of a pixel module, a flexible PCB and the supporting mechanics (a ceramic plate and an aluminium plate). The chip arrives already bump-bonded to the sensor, be it diamond or silicon. First it is glued to the ceramic plate on one side and to the PCB on the other using either Araldite 2011 or Staystik 672/472. The choice of glue was a topic of a lengthy discussion. Staystik is re-workable and has a very high thermal conductivity. The latter is important because the FE-I4 chips tend to heat up significantly and need a good heat sink. The problem is that it has a curing temperature of 160/170 °C. This temperature may cause some unwanted stress build-up between the FE-I4 and the diamond sensor due to different coefficients of thermal expansion, pulling them apart. This would disconnect the pixels, yielding large regions of the module insensitive to radiation. To avoid this, an alternative glue was tried. Araldite 2011 can be cured at lower temperatures – down to RT – but it has a lower heat conductivity. In the end Araldite is used as the safer option. However, due to the longer curing, the whole assembly process using Araldite is extended to two working days. After curing, the module is wire-bonded and attached to the aluminium plate using screws made up of a radiation-resistant PEEK plastic. They have to be tightened with a great care, because their screw head is only 0.2–0.6 mm away from the sensor edge – the sensor displacement tolerance during gluing is of the order of 0.5 mm. Finally, the module is put in an aluminium carrier which protects

206 it from mechanical damage or electrostatic discharges.

207 **1.3.2 Testing**

208 The modules are tested in the lab using an RCE readout system and a moving stage
209 with two degrees of freedom. They are placed onto the stage and connected to the
210 readout system and the power supplies. After ensuring the low- and high voltage
211 connectivity they are checked for the signal connectivity. If everything is operational,
212 a series of automated tests is run. Each of these tests calibrates a certain value within
213 a pixel, whether it is the signal threshold or the value for integrated charge. These
214 are tuned in a way that the response to a predefined calibration signal is uniform for
215 all pixels across the sensor. This procedure is referred to as *tuning*.

216 When the modules are tuned, they are tested using a ^{90}Sr radioactive source. Two
217 things are checked: 1) operation of all pixels and 2) sensor efficiency. The first test
218 is carried out by moving the module slowly under the source while taking data so
219 that the whole surface is scanned uniformly. The resulting occupancy map reveals
220 any pixels that are not electrically coupled to the sensor via bump bonds. This is an
221 important step in the DBM QC procedure, because it turned out that a significant
222 portion of the flip-chipped diamond sensors exhibited very poor connectivity. The
223 disconnected regions on the faulty modules ranged anywhere from 0.5–80 % of the
224 overall active surface. In two cases the sensor was even completely detached from the
225 chip. Therefore the pixel connectivity turns out to be the most important qualification
226 factor in the QC procedure. Unfortunately the only way to check it at the moment is
227 to fully assemble a module and test it using a radioactive source. If the module turns
228 out to be of poor quality, it is disassembled and sent for rework. The turnover time
229 of this operation is of the order of one month, which affected the DBM installation
230 schedule significantly.

231 Only the modules that passed the pixel connectivity test undergo the second
232 test stage in which the sensor’s efficiency was estimated. A scintillator is placed
233 underneath the module and is used as a trigger. A particle that crosses the DBM
234 module and hits the scintillator, triggers the module readout. In the end, the number
235 of triggers is compared to the number of hits/clusters recorded by the module. The
236 resulting ratio gives an estimate of the sensor’s detection efficiency. The real sensor
237 efficiency can only be measured in a particle beam and using a beam telescope as a
238 reference detector. Nonetheless, the *pseudo-efficiency* gives a rough estimate of the
239 sensor’s quality.

240 The results for the DBM QC are shown in section 1.4. All in all, 79 modules went
241 through the QC procedure – 43 diamond modules and 36 silicon modules, 12 of the
242 latter only for testing purposes. Figure 1.6 shows their production with time. 18
243 diamond modules and 6 silicon modules were in the end chosen to be made up into
244 DBM telescopes and installed into ATLAS.

245 A very important issue is the so called erratic current. This term describes the
246 leakage current in a pCVD diamond that becomes unstable. It can develop gradually

1.3. MODULE ASSEMBLY AND QUALITY CONTROL

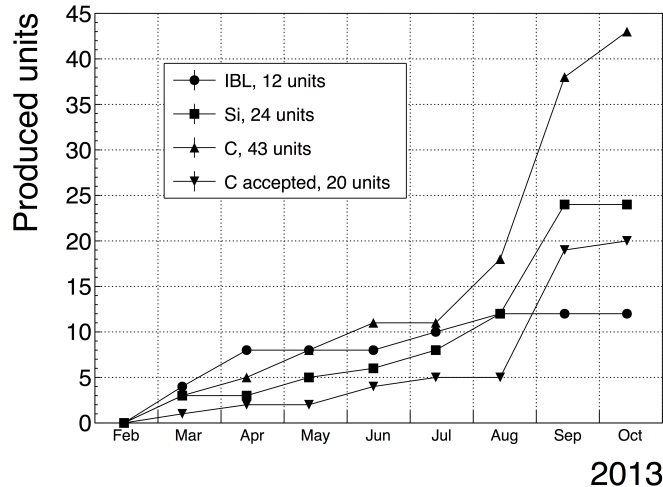


Figure 1.6: Module production with time

or can be triggered with a β source. Spikes appear in the otherwise stable leakage current. They can be up to three orders of magnitude higher than the base current. Sometimes the current also suddenly increases for a few orders of magnitude and stays at that level (e.g. from the initial 1 nA to 3 μ A). The amplitude differs in magnitude from sensor to sensor. This effect is still not fully explained, but the hypothesis is that the charges find a conductive channel along the grain boundaries, causing discharges. These discharges are picked up by the pixel amplifiers in the FE-I4. A single discharge can trigger a group of up to \sim 500 pixels, resulting in a *blob* on the detector occupancy map. Sometimes the conductive channel stays in a conductive state, making one or more pixels always to fire. These pixels only use the bandwidth of the readout channel, so they have to be masked out during measurements.

1.3.3 Installation and commissioning

The DBM modules that passed the QC tests were assembled into telescopes – sets of three modules one behind the other with a spacing of 50 mm. Of the 18 diamond and 6 silicon modules, 6 diamond and 2 silicon modules were built. A special care was taken when choosing the sets of three diamonds. The modules with a similar pseudo-efficiency, leakage current, maximum stable high voltage and shape of disconnected regions were grouped together. After assembly into telescopes, the modules were tested for their connectivity. Then the high voltage was applied and the leakage current was observed. This was an important point to check because all three modules shared the same high voltage channel. Any instabilities on one of the modules would cause problems on the other two. This would for instance happen if one of the modules had a much lower breakdown voltage.

Due to time constraints, the telescopes were not built at the same time but instead the production was pipelined. As soon as two telescopes were ready, they were transported to Point 1 – the site where parts of the ATLAS detector were being put

273 together. There they were prepared for installation onto the pixel detector struc-
274 ture that had been extracted from ATLAS due to pixel detector commissioning. The
275 commissioning was nearing completion, so the technicians were preparing the detec-
276 tor for re-insertion. The cylindrical structure was being closed off by four new service
277 quarter-panels (nSQPs). This meant that with every day the access to the place
278 of installation of the DBM was more difficult. The first two telescopes were still put
279 into place when only one nSQP was in place. This allowed the installation process
280 to be carried out from both sides. This proved to be helpful, because the process
281 was lengthy and had to be done with great precision. It involved tightening several
282 screws on both sides of the telescopes, adding thermal paste on the aluminium joints
283 and removing the protective covers, revealing the fragile wire bonds. At the same
284 time the surrounding electronics and cables had to be left untouched. The lessons
285 learnt with the first part of the installation were helpful when installing the other tele-
286 scopes. The last two were fitted onto the structure when three nSQPs were already
287 in place, leaving only a narrow opening for access. The whole procedure was carried
288 out blind. After every installation, the telescopes were tested again. First, the low
289 voltage connectivity was checked and a set of tests was run on the FE-I4 front-end
290 chips. An eye diagram was made to estimate the quality of the signal transmission.
291 Then a ^{90}Sr source was used to perform a source test on three modules at the same
292 time. Leakage current was observed during the source test. The final test included
293 running four telescopes (all on one side) at a time. All the tests were successful and
294 the DBM was signed off.

295 1.4 Performance results

296 This section gives an overview of the performance results of the DBM modules
297 achieved during the QC and the test beam campaign. The source tests were per-
298 formed to check for disconnected regions in the sensors and to measure the diamond's
299 pseudo-efficiency. Only the modules with minimal disconnected regions and maxi-
300 mum pseudo-efficiency were chosen for installation.

301 1.4.1 Source tests

302 All modules went through the same procedure when tested using a ^{90}Sr source – to
303 check for disconnected regions and to measure the pseudo-efficiency.

304 The setup consisted of a placeholder for the ^{90}Sr source, an X-Y moving stage
305 with a holder for the module and a scintillator with a photomultiplier placed below
306 the source and the module. The scintillator was used as a trigger – when it detected a
307 particle, it triggered the readout of the module. If the module was placed in between
308 the source and the scintillator, the particle had to traverse the module to hit the
309 scintillator. Therefore, in the case of a module with a 100 % efficiency the triggered
310 data read out by the module would need to contain at least one hit in the module. In
311 reality the β particles scatter around the setup and sometimes hit the scintillator from

1.4. PERFORMANCE RESULTS

312 other directions, without impinging the module. This produces empty triggers. The
313 phenomenon sets the limitation of measuring with a radioactive source as compared
314 to the measurements in a test beam, in which the particles in principle always travel
315 in one direction and their scattering is minimal.

316 The test for disconnected regions was carried out by moving the module under the
317 source in X and Y direction so that the exposure over the whole plane was uniform.
318 This resulted in an occupancy scan seen in figures 1.7a and 1.7b. The silicon module
319 had a very uniform occupancy plot. So much so that the features of the overlaying
320 flexible PCB can be observed. The rectangular shadows are the passive components
321 whereas the lines are the traces in the PCB. Furthermore, a circular-shaped edge of
322 the PCB can be seen on the bottom right side of the plot. These darker areas are
323 such because fewer electrons can penetrate the material with a high density. In the
324 case of the diamond, the features of the PCB can be observed as well, but are much
325 less distinguishable. In principle, the plot is much more granulated – less uniform.
326 This high variance in the diamond’s detection ability is due to the grain boundaries
327 in the pCVD material which trap the drifting charges, rendering some regions much
328 less efficient.

329 The pseudo-efficiency test was carried out by placing the module directly below
330 the source and collimating the particles so that their trajectory was impinging the
331 module in the middle. For every trigger by the scintillator, a script checked whether
332 there was a hit recorded in the module or not. The resulting ratio between the
333 number of triggers and number of hits recorded in the module is a pseudo-efficiency
334 – an estimation of the sensor’s efficiency. It cannot give a precise value due to the
335 triggers produced by scattered particles, but at least gives a rough estimate.

336 Figure 1.8a shows the distribution of disconnected regions across all tested mod-
337 ules. Silicon modules were performing as expected, with a minimum number of dis-
338 connected pixels. The majority of the silicon modules yielded the pseudo-efficiency
339 of $(94.3 \pm 0.2) \%$. Silicon sensors being 99.99 % efficient, this value was underesti-
340 mated by about 5 %. The measured pseudo-efficiency of the diamond modules was
341 $(65 \pm 7) \%$, with outliers down to 10 %. The value depended on the diamond quality,
342 the set threshold and the applied bias voltage. The latter two settings were varied to
343 check the behaviour of the modules under various conditions.

344 1.4.2 Test beam results

345 The first two assembled prototype DBM modules, MDBM-01 and MDBM-03, were
346 tested at DESY, Hamburg, in a test beam facility. The aim of the measurements was
347 to measure their efficiency, the spatial distribution of the efficiency and the effect of
348 the beam on the disconnected regions. A silicon module MSBM-02 was measured to
349 crosscheck the measurements. Since the silicon module is almost 100 % efficient, it
350 was used as an “anchor” – the efficiency of the diamond module was measured relative
351 to that of the silicon module. Two beam telescopes were used as reference systems:
352 Kartel [], built by JSI institute from Ljubljana, and EUDET Aconite []. Both are

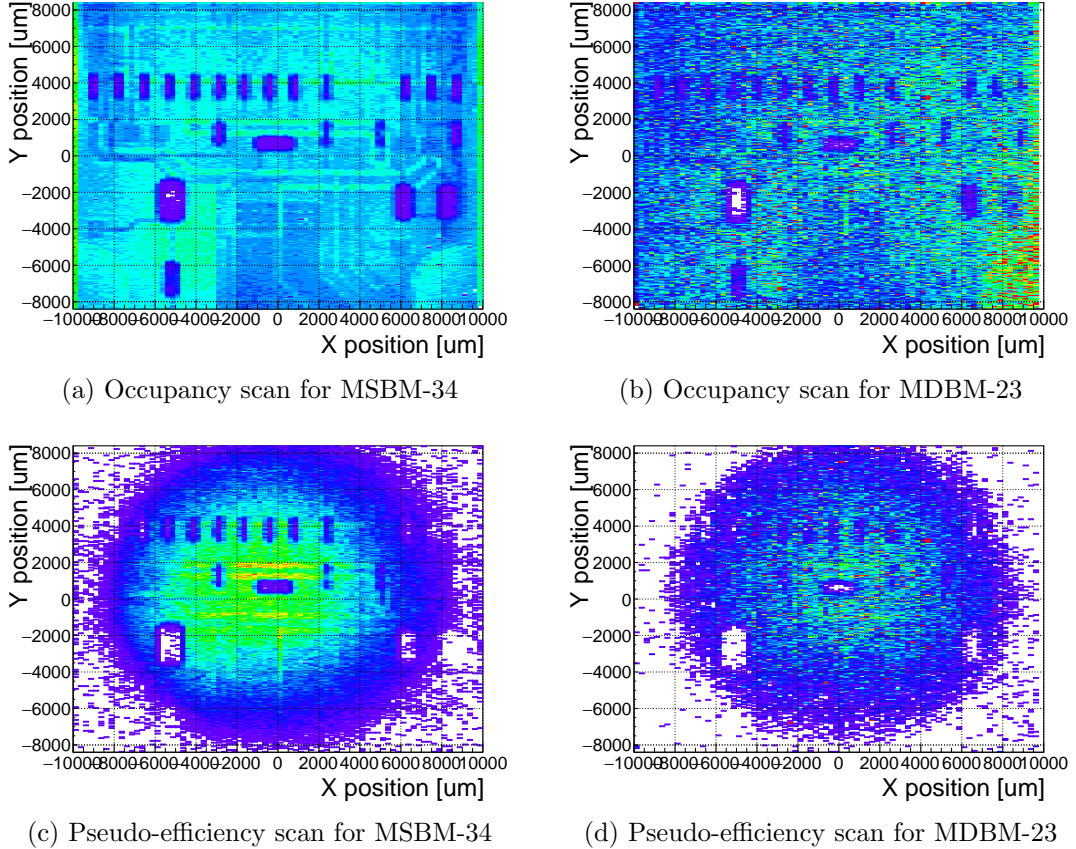


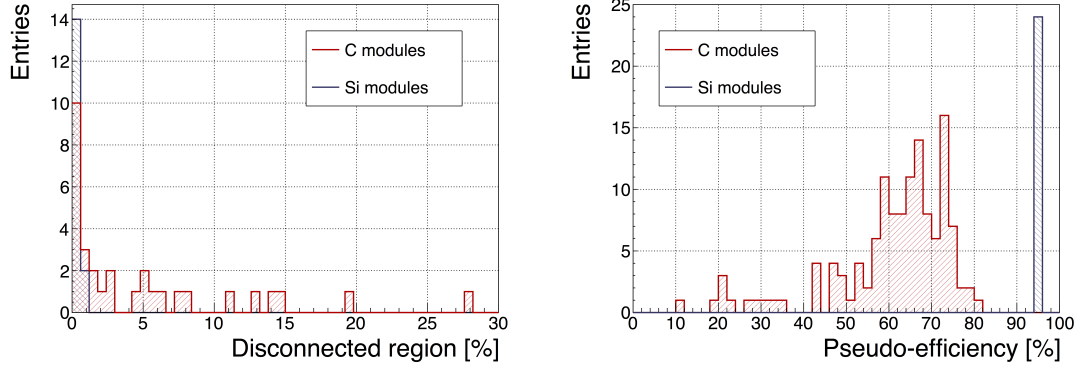
Figure 1.7: Occupancy and pseudo-efficiency scans for the silicon (left) and diamond sensor (right) to check for disconnected regions and estimate the sensor’s efficiency. Shadows of the electronic components are clearly visible because fewer electrons were able to traverse through such a higher amount of material.

353 instrumented with six Mimosa26 pixel planes and capable of tracking particles with
354 a $2 \mu\text{m}$ pointing resolution.

355 The test beam prototypes did not meet the acceptance criteria for production
356 DBM modules in the following areas: first, the stated CCDs were slightly below
357 $200 \mu\text{m}$, which would be the DBM minimum. Secondly, the applied bias voltages
358 ranged from $1\text{--}2 \text{ V}/\mu\text{m}$. In addition, the threshold cut could only be set to 1500 elec-
359 trons, which is higher than the DBM minimum (1000 e). Nonetheless, the resulting
360 module efficiencies were still in the range between 70–85 %.

361 To analyse the test beam data, Judith [] software framework was used. Judith is
362 capable of synchronising data streams from several detector systems only connected
363 via a trigger system, reconstructing tracks and calculating efficiency for the DUTs. It
364 was also used to reconstruct and analyse the acquired Kartel test beam data together
365 with the silicon and diamond module as DUTs. A sample of the analysed data is
366 shown in figures 1.9a and 1.9b.

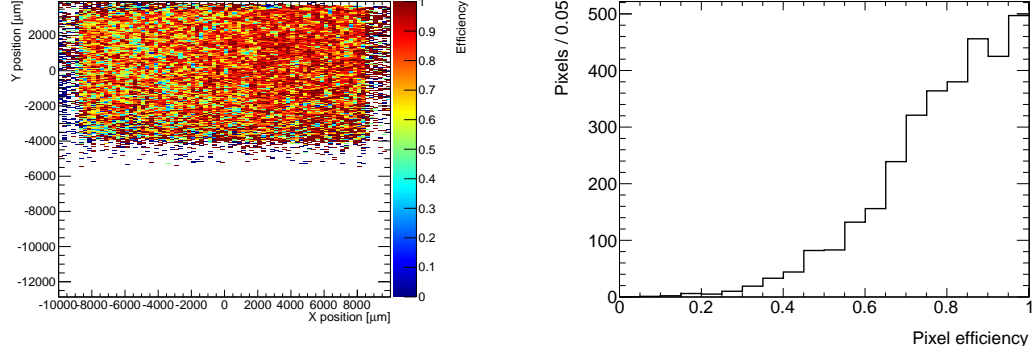
1.5. OPERATION



(a) Disconnected regions for all modules derived from the occupancy scans

(b) Pseudo-efficiencies for all modules at various threshold and voltage settings

Figure 1.8: Measurements of pseudo-efficiency and disconnected regions for all modules that went through the QC procedure



(a) This is an efficiency distribution. Each bin corresponds to a single pixel. The triggering scintillator of the Kartel telescope was smaller than the DUT. Hence, the recorded hits can only be seen in the top half of the sensor.

(b) Pseudo-efficiencies for all modules at various threshold and voltage settings

Figure 1.9: An efficiency study of a prototype DBM diamond module in a test beam. The statistics are low (~ 10 hits/pixel) as the data was collected during a short run.

367 1.5 Operation

368 1.5.1 Positioning

369 The DBM is placed in the forward region of the ATLAS detector, very close to the
 370 beam pipe (see figure 1.11). The mechanical structure that holds the sensor planes is,
 371 due to its shape, referred to as a DBM telescope. A telescope is a system that consists
 372 of several pixel sensors placed in series one behind the other. Each DBM telescope
 373 houses three diamond pixel modules. Eight DBM telescopes reside approximately
 374 1 m away from the collision region, four on each side. They are tilted with respect



Figure 1.10: This photo highlights four telescopes installed onto the nSQPs and around the pipe

375 to the beam pipe for 10° . This is due to a specific phenomenon connected to erratic
376 (dark) currents in diamond. Studies have shown [1] that the erratic leakage currents
377 that gradually develop in diamond can be suppressed under certain conditions. For
378 instance, if a strong magnetic field is applied perpendicular to the electric field lines
379 in the diamond bulk, the leakage current stabilises [2]. The DBM was designed to
380 exploit this phenomenon. The magnetic field lines in the ATLAS experiment are
381 parallel to the beam. Hence, an angular displacement of the sensor with respect to
382 the beam allows for the leakage current suppression. However, the DBM telescopes
383 still need to be directed towards the interaction region. Taking these considerations
384 into account, a 10° angle with respect to the beam pipe was chosen. The influence
385 of the magnetic field on the particle tracks at this angle is very low as the field lines
386 are almost parallel to the tracks. The tracks are therefore straight, which reduces the
387 track reconstruction complexity.

388 1.5.2 Data taking during collisions

389 The DBM has been commissioned in ATLAS and is now taking data. Several issues
390 still need to be resolved regarding the readout systems. Unfortunately, due to issues
391 with the low voltage power supply regulators, six out of 24 modules were damaged
392 during operation: four silicon and two diamond modules. The system configured

1.5. OPERATION

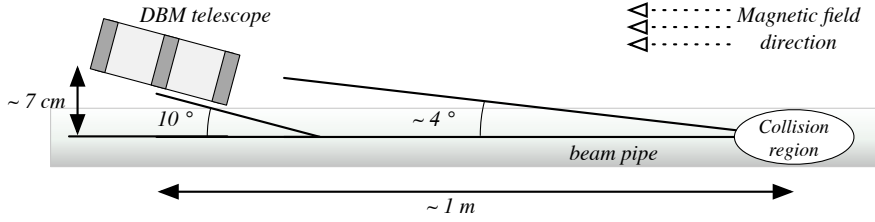


Figure 1.11: Position of the DBM in the ATLAS experiment

FIGURE PLACEHOLDER

Figure 1.12: Occupancy of individual modules during collisions. Only 16 modules were taking data.

393 the modules into an unsteady state whereby they drew twice as much current as the
 394 allowed maximum. This current most probably fused the wire bonds within minutes.
 395 This has left only five diamond telescopes fully operational. The preliminary data
 396 obtained using the remaining telescopes show that the background rejection could
 397 indeed work.

398 The first step of the system test was to take data during collisions and check
 399 the occupancy in the individual modules. The occupancies were plotted side by side
 400 for comparison. Figure 1.12 shows some of the occupancy values. At the time, the
 401 readout system was not yet configured to read out all telescopes in parallel.

402 The second step was to test the detector's capability of particle tracking. Only one
 403 telescope was used to take data with the beam. If all three planes of the telescope
 404 were hit during a bunch crossing, a linear line was fitted to the hits. This line
 405 represented the particle's trajectory. It was projected towards the interaction point.
 406 Two parameters were calculated where the line is the closest to the interaction point:
 407 the radial distance and the longitudinal distance between the line and the interaction
 408 point (see figure 1.13). This was done for the events with two colliding bunches as
 409 well as for events with only one, non-colliding bunch. The tracks recorded during
 410 the events with two colliding bunches could either come from the collisions or could
 411 be background scattering. Tracks recorded during a non-colliding bunch, on the
 412 other hand, are definitely background particles since, in principle, there should be no
 413 collisions taking place.

414 A comparison of the data acquired (see figures 1.14a and 1.14b) showed that, for
 415 the colliding bunches, the majority of the reconstructed tracks had the origin in the
 416 interaction point, with an expected spread in Z and R . For non-colliding bunches,
 417 the distribution is more spread out. In the Z_0 plot the distribution has one peak in
 418 the middle, which means that the empty RF buckets still held some particles. The
 419 two peaks on the sides, however, show that a significant number of tracks had their
 420 origin at the radius of the beam pipe. Therefore these tracks were made by stray
 421 protons colliding with the beam pipe. These collisions are unwanted as they do not

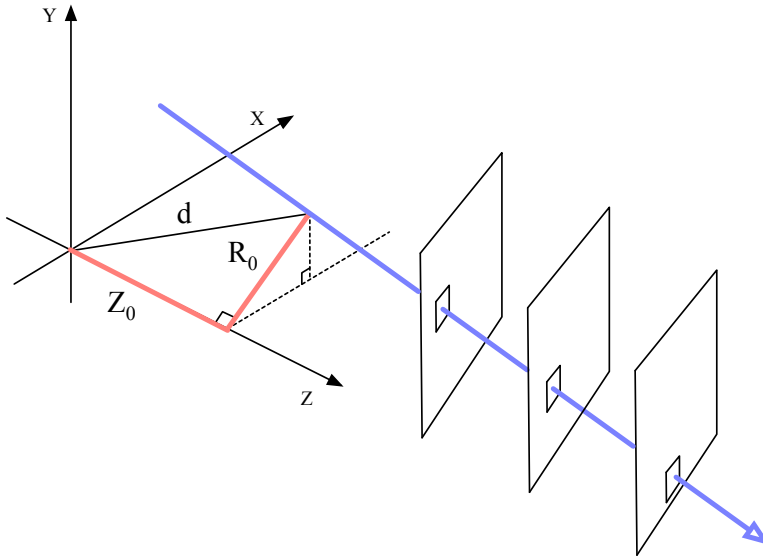


Figure 1.13: A diagram showing the radial distance R_0 and longitudinal distance Z_0 of the trajectory from the interaction point at the minimal distance d . Z is the axis along the beam line. Three module planes intercept a particle and reconstruct its trajectory.

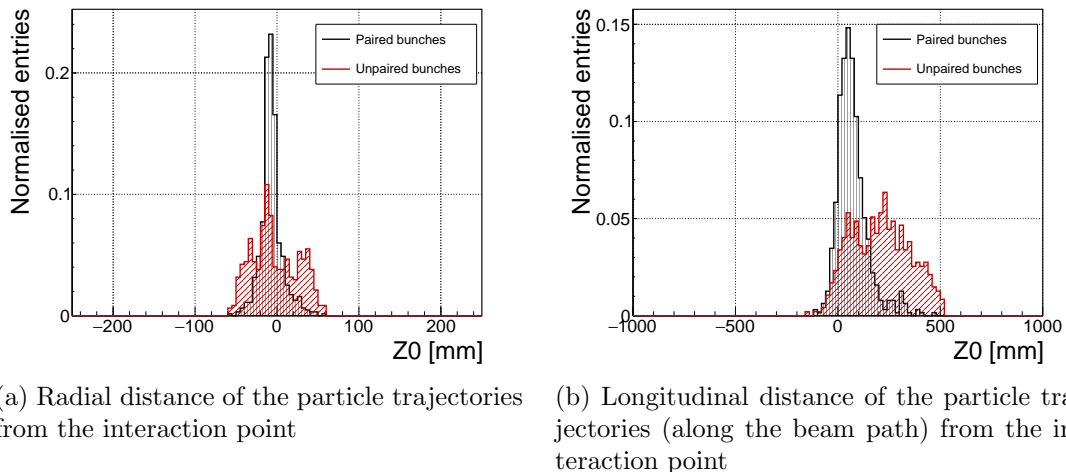


Figure 1.14: These two plots show two parameters of particle tracks recorded by one of the DBM telescopes: radial and longitudinal distance of the projected tracks from the interaction point.

⁴²² produce any meaningful physics while still damaging the ATLAS detector by means of the scattered radiation.

424 1.6 Conclusion

425 The Diamond Beam Monitor has been designed as an upgrade to the existing lu-
426 minosity detectors in the ATLAS experiment. It is the first diamond pixel tracking
427 detector installed in a high-energy physics experiment. The pixelated front-end elec-
428 tronic chips ensure precise spatial detection of the charged high-energy particles.
429 The projective geometry allows for particle tracking and background rejection. The
430 detector is placed in a high-radiation forward region of the experiment. Therefore,
431 radiation hardness of the chosen pCVD diamond sensors is an important requirement.
432 The tests carried out in the test beam and in the laboratory confirmed that enough
433 detector-grade DBM modules have been built to be installed in the experiment. The
434 DBM is now running in ATLAS during collisions. Further improvements have to be
435 made on the readout firmware before it is included in the main readout stream.

⁴³⁶ **Bibliography**